THE JOURNAL OF PHYSICAL CHEMISTRY Letters

Letter

Cite This: J. Phys. Chem. Lett. 2019, 10, 2031−2036

pubs.acs.org/JPCL

Effect of Functional and Electron Correlation on the Structure and Spectroscopy of the $Al_2O_3(001)-H_2O$ Interface

Published as part of The Journal of Physical Chemistry virtual special issue "Hai-Lung Dai Festschrift".

Mark J. DelloStritto,[†,‡] Stefan M. Piontek,[†,‡] Michael L. Klein,[†,¶,‡] and Eric Borguet*[,†,‡]

[†]Department of Chemistry, [‡]Center for Complex Materials from First-Principles, and [¶]Institute for Computational Molecular Science, Temple University, Philadelphia, Pennsylvania 19122, United States

Supporting Information

ABSTRACT: Oxide−water interfaces are ubiquitous, with many applications in industry and the environment, yet there is a great deal of controversy over their properties and microscopic structure. This controversy stems, in part, from the unique H-bond networks formed at different surface terminations and mineral compositions. Density functional theory simulations of these interfaces require an accurate description of both the oxide mineral and water in diverse H-bond environments. Thus, herein we simulate the $Al_2O_3(001)-H_2O$ interface using the PBE, PBE-TS, RPBE, SCAN, and HSE06-TS functionals to determine how calculated interfacial properties depend on the choice of functional. We find that the structure of the first few layers of water at the surface is determined by electron correlation in a way that cannot be approximated using semiemipirical van der Waals corrections. Of the functionals investigated, we find that SCAN yields the most accurate interfacial structure, dynamics, and sum frequency generation spectrum. Furthermore, SCAN leads to a reduction in the order of the 2D H-bond network of water at the alumina surface predicted by GGA functionals, leading to a significant decrease in the anisotropy of the diffusion coefficient at the surface. We emphasize the importance of using a functional which accurately describes electron correlation for more complex oxides, such as transition-metal oxides, where electron correlation may play an even greater role in determining the structure and dynamics of the oxide−water interface.

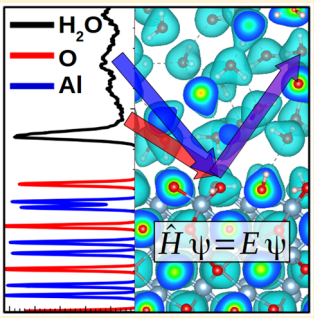

Oxide−water interfaces are ubiquitous in physics, chemistry, and environmental science and have applications in climate science,[1] ocean chemistry,[2] catalysis,[3,4] and gas-sensing.[5] As oxide minerals are nearly always covered by H_2O or hydroxyl groups in ambient conditions, these processes are driven by the structure and dynamics of the interfacial H-bond network. The role of the H-bond network is considered essential in describing the change in dissolution rate of silica with the addition of ions,[6,7] and the frustration of confined water can drive charge-transfer processes in layered oxides.[8]

Theoretical models are often necessary to understand the characteristics of H-bond networks, yet an accurate description of H-bond interactions remains elusive because of their complexity and dynamic nature. While techniques such as X-ray reflectivity (XRR)[9] can measure average atomic positions and sum frequency generation (SFG)[10] can probe the interfacial vibrational spectrum, they are limited when it comes to revealing the atomistic details of H-bond networks. The low charge density of H makes it essentially invisible to X-rays; inelastic neutron scattering suffers from poor statistics at interfaces, and inferring H-bond structure from the vibrational spectrum is difficult with little a priori knowledge of the interfacial structure. Thus, theory and simulation are necessary for a complete understanding of the interfacial H-bond network.

Density functional theory (DFT) is the only theoretical method that is both efficient and accurate enough to describe H-bond interactions in bulk-like systems with hundreds of atoms. Yet researchers have struggled to develop functionals which yield accurate H-bond interactions. Functionals based on the generalized gradient approximation (GGA), such as PBE[11,12] and BLYP,[13,14] have been well-established standards for years, but they ultimately fail for oxide−water interfaces. The PBE functional is notorious for overstructuring water,[15] and while BLYP significantly improves the structure of water,[15] it does not perform well for solids.[16] Indeed, this is a common problem among GGA functionals: they are either biased toward free-atom energies or work well for densely packed solids, but do not perform well for both.[17] Instead, one might hope that a meta-GGA functional would have a broader range of accuracy and therefore be more applicable for oxide−water interfaces. The recently developed SCAN meta-GGA functional[18] is designed to reproduce a number of exact constraints and appropriate norms and as a consequence yields an excellent description of the properties of liquid water[19] as well as accurate structures and energies of a diverse array of

Received: January 3, 2019
Accepted: March 26, 2019

DOI: 10.1021/acs.jpclett.9b00016
J. Phys. Chem. Lett. 2019, 10, 2031−2036

systems.[20] Therefore, SCAN may be the most promising meta-GGA functional for oxide−water interfaces.

We have evaluated the ability of DFT to yield accurate structures and dynamics of oxide−water interfaces by comparing the performance of several functionals at the alumina−water interface. Previous work has shown surprising results at the alumina surface,[21] where the RPBE functional fails to yield accurate interfacial structures despite the fact that it yields an accurate model of liquid water. In addition, it has been shown that the choice of functional strongly impacts the SFG peak positions and intensities at the air−water interface, especially the intensity and low-frequency tail of the O−H stretching peak.[22]

We expand upon this work by studying GGA, meta-GGA, and hybrid functionals in order to determine how different aspects of density functionals impact both the structure and dynamics of the alumina−water interface. Alumina has a relatively low dissolution rate[23] and generally large pK_a's for surface OH groups (aluminols),[24] yielding stable surface structures which change little over the course of an experiment. We choose to study the (001) surface as it has a relatively simple, well-characterized structure: it is atomically flat and is completely hydroxylated by a single species of OH group.[25−27] Alumina is a relatively simple oxide, unlike transition-metal oxides, and so does not require any semiempirical corrections (e.g., Hubbard U or exact exchange). Finally, at a positively charged or near-neutral interface, although the intensity of the spectrum can change greatly with the addition of anions which compensate the surface charge, the overall shape of the SFG spectrum changes little.[28] Thus, while surface charge can strongly impact water orientation and thereby the contribution of the diffuse layer to the SFG spectrum,[29] at a near-neutral SFG spectra we are confident that the relevant features of the spectrum can be accurately modeled using AIMD simulations, which are limited in size and can show the contribution of only the first few nanometers of interfacial water to the SFG spectrum.[28] Alumina is therefore an ideal test system for ab initio methods, and despite the relative simplicity of the Al_2O_3(001)−H_2O interface, many of its properties are not fully understood. There is still some disagreement in the origin of the features of the SFG spectrum,[30,31] namely, the molecular origin of the two main O−H stretching peaks, and it is still not clear why the vibrational relaxation rate differs between surface terminations.[32] Therefore, while alumina is a relatively simple bulk material with a stable, neutral surface at pH 6, there are still open questions regarding many of its properties.

We modeled the Al_2O_3(001)−H_2O interface using an O-terminated six-layer Al_2O_3 slab[33] cleaved from the ideal crystal using Materials Studio v7.0.[34] We passivated both surfaces with H atoms as dissociative adsorption of H_2O is favored on the (001) surface.[25,26,35] We expanded the unit cell of the alumina surface to get final dimensions of (8.243 × 9.518 × 20.0 Å^3), corresponding to a surface with 12 aluminols (∼15/nm^2).

To overcome sampling problems associated with DFT-MD, we ran five independent simulations. The cells were initialized using PACKMOL[36] with a 10 nm vacuum gap and were equilibrated using classical MD (CMD) with ClayFF[37] in LAMMPS.[38] We ran CMD in the *NVT* ensemble at 423 K for 1 ns, reduced the gap to 2 nm over 1 ns, reduced the temperature to 300 K for 1 ns, and finally equilibrated the system at 300 K for 1 ns. This procedure ensures the H_2O molecules had the freedom to find their equilibrium orientation at each alumina interface. We chose a gap of 2 nm as CMD simulations show that the oscillations in the density profile are damped within ∼1 nm for a wide range of oxide−water interfaces.[39−41] The final cell has a *z*-axis length of 35.0 Å, and we placed 52 H_2O molecules in the gap in order to achieve water densities of 0.998 g/cm^3, as calculated from the volume of the cell occupied by the H_2O molecules.

After equilibration all subsequent calculations were performed using DFT. We employed the following functionals: PBE, PBE with van der Waals (vdW) corrections using the Tkatchenko−Scheffler method (PBE-TS),[42] RPBE, SCAN, and HSE06-TS.[43] Both PBE-TS and RPBE improve the structure of water compared to PBE,[44,45] while HSE06-TS yields a highly accurate description of liquid water.[46] For all functionals except SCAN we use plane-wave-based DFT in VASP (v.5.4.4)[46−49] using the projector-augmented wave[50,51] method and Born−Oppenheimer MD (BOMD). We attempted BOMD with SCAN but found that even with a 1000 eV cutoff and a convergence criterion of 1×10^{-5} there persisted a non-negligible drift in the energy. Thus, for SCAN we used Car−Parrinello MD (CPMD) as implemented in Quantum Espresso (v.6.2.1) using HSCV norm-conserving pseudopotentials,[52] a cutoff of 90 Ry, and an electron mass of 100 au. For all nonhybrid simulations, we first relaxed the initial structures, ran *NVT* simulations until the average energy stopped changing, and then ran simulations in the *NVE* ensemble. The GGA and SCAN simulations were run for 27.5 and 20 ps, respectively. Because of the great expense of hybrid functional calculations, only one HSE06-TS simulation was run in the *NVT* ensemble for 3.5 ps in order to extract structural averages. Finally, the vSFG experimental parameters are included in the Supporting Information, as they have been described elsewhere.[32]

We find that SCAN yields significant improvements in the structure of the Al_2O_3(001)−H_2O interface, even compared to HSE06-TS, and is the only functional to yield the correct position of the first water layer at the oxide surface. We compare average O and Al positions to XRR data in Table 1,

Table 1. Average Atomic Positions (Å) along Surface Normal

atom	exptl[53]	PBE	PBE-TS	RPBE	SCAN	HSE06-TS
O−H_2O	8.15	8.38	8.34	8.53	8.12	8.24
O1	5.69	5.72	5.70	5.77	5.50	5.60
Al1	4.74	4.81	4.80	4.85	4.63	4.69
Al2	4.37	4.51	4.51	4.57	4.35	4.42
O2	3.54	3.55	3.53	3.57	3.42	3.47
Al3	2.72	2.69	2.67	2.71	2.62	2.64
Al4	2.17	2.19	2.17	2.20	2.08	2.14
O3	1.32	1.34	1.33	1.35	1.30	1.31
Al5	0.51	0.49	0.48	0.48	0.50	0.46

which shows that, compared to the GGA and HSE06-TS functionals, SCAN improves the position of the first layer of water by moving it ∼0.2 and 0.1 Å closer to the surface, respectively. The positions of the oxide atoms do not change much for each functional, with the only notable change being that the O and Al atoms in the surface layer move ∼0.1 Å into the bulk for both SCAN and HSE06-TS compared to the GGA functionals and experiment. Note that RPBE, which yields an accurate structure for bulk water, is the least accurate functional when it comes to the position of H_2O at the surface. Thus, it appears that the effects of electron correlation

DOI: 10.1021/acs.jpclett.9b00016
J. Phys. Chem. Lett. 2019, 10, 2031−2036

beyond semiempirical functionals and vdW corrections are important for studying H_2O at oxide surfaces.

The improvement in position of the first H_2O layer achieved with SCAN is due to significant changes in the H-bond strength and thereby H-bond structure in the first water layer. To investigate the changes in structure further, we list the number of H-bonds N_H donated from surface groups (s−s), from surface to water (s−w), and from water to surface (w−s) in Table 2, as well as the length of the H-bonds from surface to water (s−w) and from water to surface (w−s). When moving from PBE/PBE-TS to SCAN/HSE06-TS, there is an increase in (w−s) and (s−w) H-bonding, with a corresponding decrease in the number of (s−s) H-bonds. However, despite the fact that SCAN moves H_2O molecules closer to the surface and increases the number of surface water H-bonds, the surface water H-bonds actually increase in length [both R_H(s−w) and R_H(w−s)]. This strange behavior can be understood by measuring the orientations of surface H_2O molecules as shown in the angular distribution function (ADF) of the O−H bonds of the H_2O molecules in Figure 1. The PBE and to a lesser extent the PBE-TS functionals tend to overstructure water in the first layer at the alumina surface, yielding H_2O molecules in a rigid, 2D H-bond network with H-bonds either parallel or perpendicular to the surface plane. This 2D H-bond network yields sharp peaks in the ADF and inefficient H-bonding between H_2O and aluminols. The SCAN, RPBE, and HSE06-TS functionals all weaken the H-bonds compared to PBE,[19] causing the H_2O molecules to break some H-bonds and rotate away from the surface normal, yielding broader distributions in the ADF and allowing H_2O molecules to move closer to the surface in the case of SCAN and HSE06-TS.

Table 2. Interface H-Bond Data

	N_H(s−s)	N_H(s−w)	N_H(w−s)	R_H(s−w) (Å)	R_H(w−s) (Å)
PBE	3.81	3.31	2.9	1.88	1.68
PBE-TS	3.82	3.88	3.15	1.86	1.68
RPBE	5.46	2.88	2.72	1.96	1.74
SCAN	3.60	3.74	3.23	1.96	1.70
HSE06-TS	3.92	3.49	3.1	1.85	1.72

The breaking of the ordered, 2D H-bond network at the interface with more accurate functionals has profound consequences for interfacial water dynamics. Even though the simulations are short, we can still estimate the impact of the H-bond network by calculating the diffusion coefficient, D, of the H_2O molecules within the first water layer at the interface. While the absolute values are not very useful, it is instructive to compare the components of D in different dimensions, by calculating the slope of the mean squared displacement of each H_2O molecule along each component of the displacement. We list the ratio of each component of D to the total D for each functional in Table 3. The PBE and PBE-TS functionals yield very small relative D's in the z-direction because of the 2D nature of the H-bond network in the first layer. While SCAN and HSE06-TS both predict a smaller out-of-plane D versus in-plane D, the out-of-plane D is significantly larger than for other functionals. Thus, it appears that accounting for the effects of electron correlation, beyond semiempirical functionals and vdW corrections, is essential for yielding both accurate structure and dynamics of water at oxide surfaces.

Table 3. Diffusion Coefficient Components Relative to Total

functional	x	y	z
PBE	0.35	0.61	0.04
PBE-TS	0.57	0.32	0.11
RPBE	0.27	0.34	0.40
SCAN	0.37	0.37	0.26
HSE06-TS	0.44	0.42	0.14

On the basis of the broad applicability of SCAN and on its performance for water, we expect SCAN to improve the H-bond vibrational dynamics as well as the H-bond structure at the interface,[19,20] and so we calculate the SFG spectrum using a bond polarizability model[31] with the DFT-MD trajectories. We do not include a nonresonant contribution as the measured spectra are normalized by the nonresonant vSFG signal generated by a gold-coated α-Al_2O_3(0001) prism (Supporting Information). We plot the spectra for the SSP polarization, which primarily measures the χ_{yyz} component of the nonlinear susceptibility, for each functional compared to the experimental results in Figure 2. The spectrum consists of two main peaks, at ∼3200 and ∼3400 cm^{-1}, with the former arising

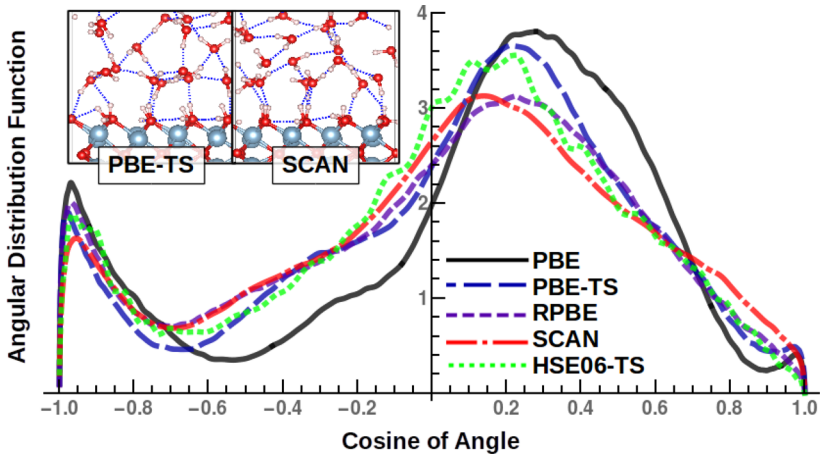

Figure 1. Angular distribution functions of the H_2O molecules in the first layer at the Al_2O_3(001) interface. The inset shows a snapshot of the PBE-TS and SCAN simulations, where we see that there are fewer in-plane water−water H-bonds when using SCAN as compared to PBE-TS.

DOI: 10.1021/acs.jpclett.9b00016
J. Phys. Chem. Lett. 2019, 10, 2031−2036

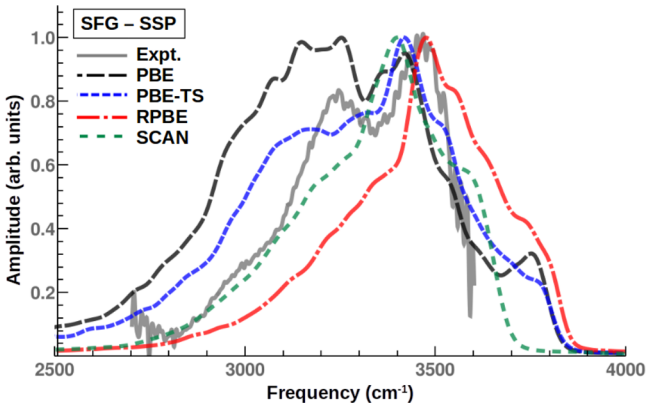

Figure 2. Calculated SFG spectra for the $Al_2O_3(001)-H_2O$ interface for each functional for SSP polarization compared to the experimental spectra. The gray line depicts the experimental spectrum.

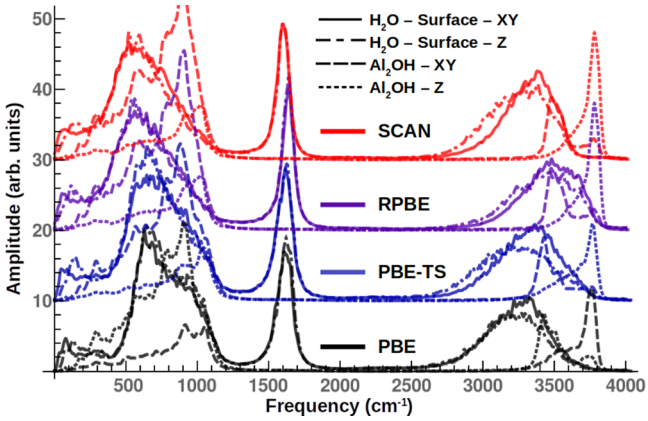

Figure 3. VDOS of the surface H_2O and aluminol groups, with the solid, dot-dashed, dashed, and dotted lines depicting the VDOS of the H_2O molecules projected along the surface plane, H_2O molecules projected along the surface normal, aluminols projected along the surface plane, and the aluminols projected along the surface normal, respectively.

mainly from interfacial H_2O while the latter has a strong contribution from in-plane aluminols (Supporting Information). This contrasts previous work ascribing the 3200/3400 cm^{-1} peaks to ice-/liquid-like bands, respectively.[54] Our assignments agree with previous DFT-MD simulations,[55] while experiments cannot directly distinguish the different OH groups at the interface.[56,57] As we go from more to less structured water while moving from PBE to SCAN, the 3200 cm^{-1} peak decreases in intensity. This is consistent with changes in the intensity of the 3400 cm^{-1} band seen with different functionals at the air-water interface. Adding dispersion corrections results in less structured water, resulting in a decreased contribution to the 3400 cm^{-1} from water beyond the first layer.[22] The RPBE functional is blue-shifted with respect to experiment, with greater weight at higher frequencies not present in the experimental spectrum. The SCAN spectrum has a shape similar to RPBE but is red-shifted to more accurate frequencies.

Finally, to understand the origin of the SFG spectral features and how they are affected by the choice of functional, we calculate the vibrational spectrum of the interface as represented by the vibrational density of states (VDOS) of the surface H_2O molecules and aluminols for each functional. While we can decompose the SFG spectrum in terms of different molecules, we cannot determine the molecular orientations from SFG alone, and so in Figure 3 we decompose the aluminol VDOS in terms of in-plane and out-of-plane contributions. From Figure 3 we see that the ~3200 cm^{-1} peak in the SFG spectrum arises primarily from H_2O modes while the ~3400 cm^{-1} peak has a strong contribution from in-plane aluminols. Note that while both RPBE and SCAN lead to a blue-shift in the surface modes compared to PBE and PBE-TS, RBPE overcorrects the vibrational modes of H_2O, vastly overestimating the weight of the VDOS at higher frequencies. Here we see the importance of a general functional with wide applicability for oxide interfaces: the presence of both constrained H-bonds on the oxide surface and H-bonds in liquid water precludes essentially any GGA functional from accurately describing the alumina–water interface. Any correction which weakens the PBE H-bonds, thereby improving the structure of water, will lead to a much smaller blue-shift in the surface modes, as the intrasurface H-bond lengths are constrained by the oxide lattice. Thus, while empirical corrections to GGA functionals can yield improved interfacial structures, such corrections are not guaranteed to yield the accurate relative frequencies of the H_2O and aluminol modes and can even overcorrect and yield qualitatively incorrect spectra.

In conclusion, we find that an accurate model of electron correlation is essential for simulating water at an oxide surface terminated with hydroxyl groups, even for a relatively simple oxide such as alumina. The structure of the water at the interface is determined by intermolecular interactions which cannot be approximated using semiempirical methods such as TS-vdW corrections or even including exact exchange. These interactions can often lead to counterintuitive results, such as H_2O molecules moving closer to the interface while also lengthening water–surface H-bonds. We also find that the use of SCAN is important for the dynamics at the interface, with SCAN being the only functional investigated to yield the proper widths and intensities of the peaks in the SFG spectrum. While the RPBE functional improves the widths of the peaks and leads to a blue-shift in the VDOS, it overcorrects and results in erroneously large amplitudes at higher frequencies in the SFG spectrum. Thus, at oxide–water interfaces it is not enough that the functional simply yields an accurate structure of water. It must also accurately represent the oxide interface and interactions between the solid and the liquid. Hence, the functional must have broad applicability over a wide range of structures and molecular orientations. We find that the SCAN functional is the only one tested which possesses such a broad applicability and is therefore able to yield accurate structures and dynamics at the $Al_2O_3(001)-H_2O$ interface. In addition, SCAN improves the interfacial structure compared to the much more expensive hybrid functional HSE06-TS, thereby offering a more accurate and cheaper alternative to the current best performing functional for the $Al_2O_3(001)-H_2O$ interface. This study highlights the importance of proper functional choice for all aqueous interfaces, and in particular for water at the surface of complex oxides such as the isostructural hematite, which shows marked differences in interfacial structure,[33] and perovskites where strong electron correlation may play an even greater role in determining the structure and dynamics of adsorbed water.[58]

DOI: 10.1021/acs.jpclett.9b00016
J. Phys. Chem. Lett. 2019, 10, 2031–2036

■ ASSOCIATED CONTENT

Supporting Information

The Supporting Information is available free of charge on the ACS Publications website at DOI: 10.1021/acs.jpclett.9b00016.

Radial distribution function, component decomposition and depth dependence of SFG spectrum, polarizability parameters, sample preparation experimental details, and SFG optical setup (PDF)

■ AUTHOR INFORMATION

Corresponding Author

*E-mail: eborguet@temple.edu.

ORCID

Mark J. DelloStritto: 0000-0002-0678-5860

Stefan M. Piontek: 0000-0001-9564-6258

Notes

The authors declare no competing financial interest.

■ ACKNOWLEDGMENTS

This research includes calculations carried out on Temple University's HPC resources and thus was supported in part by the National Science Foundation through major research instrumentation Grant Number 1625061 and by the US Army Research Laboratory under Contract Number W911NF-16-2-0189. This work was funded in part by the Center for the Complex Materials, an Energy Frontier Research Center funded by the US DOE, Office of Science, Basic Energy Sciences under Grant No. DE-SC0012575 and in part by the Computational Chemical Center: Chemistry in Solution and at Interfaces under DOE Award DE-SC0019394. The authors acknowledge the National Science Foundation for supporting the experimental results presented in this work (NSF Grant CHE 1337880). We thank Xifan Wu at the Physics Department at Temple for useful discussions on SFG spectroscopy and for help and advice on running simulations with VASP with SCAN.

■ REFERENCES

(1) Berner, R. A. Weathering, plants, and the long-term carbon cycle. *Geochim. Cosmochim. Acta* **1992**, *56*, 3225−3231.

(2) Stumm, W. *Chemistry of the solid-water interface: Processes at the mineral-water and particle-water interface in natural systems.*; John Wiley and Sons, Inc.: New York, NY, 1992.

(3) Hoffmann, M. R.; Martin, S. T.; Choi, W.; Bahnemann, D. W. Environmental Applications of Semiconductor Photocatalysis. *Chem. Rev.* **1995**, *95*, 69−96.

(4) Suntivich, J.; May, K. J.; Gasteiger, H. A.; Goodenough, J. B.; Shao-Horn, Y. A Perovskite Oxide Optimized for Oxygen Evolution Catalysis from Molecular Orbital Principles. *Science* **2011**, *334*, 1383−1385.

(5) Wang, C.; Yin, L.; Zhang, L.; Xiang, D.; Gao, R. Metal Oxide Gas Sensors: Sensitivity and Influencing Factors. *Sensors* **2010**, *10*, 2088−2106.

(6) Dove, P. M. The dissolution kinetics of quartz in aqueous mixed cation solutions. *Geochim. Cosmochim. Acta* **1999**, *63*, 3715−3727.

(7) Dewan, S.; Yeganeh, M. S.; Borguet, E. Experimental Correlation Between Interfacial Water Structure and Mineral Reactivity. *J. Phys. Chem. Lett.* **2013**, *4*, 1977−1982.

(8) Remsing, R. C.; Klein, M. L. Solvation dynamics in water confined within layered manganese dioxide. *Chem. Phys. Lett.* **2017**, *683*, 478−482.

(9) Fenter, P.; Sturchio, N. C. Mineral-water interfacial structures revealed by synchrotron X-ray scattering. *Prog. Surf. Sci.* **2004**, *77*, 171−258.

(10) Shen, Y. R. *The Principles of Nolinear Optics*; Wiley, 2003.

(11) Perdew, J. P.; Burke, K.; Ernzerhof, M. Generalized Gradient Approximation Made Simple. *Phys. Rev. Lett.* **1996**, *77*, 3865−3868.

(12) Perdew, J. P.; Burke, K.; Ernzerhof, M. Erratum: Generalized Gradient Approximation Made Simple. *Phys. Rev. Lett.* **1997**, *78*, 1396−1396.

(13) Becke, A. D. Density-functional exchange-energy approximation with correct asymptotic behavior. *Phys. Rev. A: At., Mol., Opt. Phys.* **1988**, *38*, 3098−3100.

(14) Lee, C.; Yang, W.; Parr, R. G. Development of the Colle-Salvetti correlation-energy formula into a functional of the electron density. *Phys. Rev. B: Condens. Matter Mater. Phys.* **1988**, *37*, 785−789.

(15) Lin, I.-C.; Seitsonen, A. P.; Tavernelli, I.; Rothlisberger, U. Structure and Dynamics of Liquid Water from ab Initio Molecular Dynamics-Comparison of BLYP, PBE, and revPBE Density Functionals with and without van der Waals Corrections. *J. Chem. Theory Comput.* **2012**, *8*, 3902−3910.

(16) Paier, J.; Marsman, M.; Kresse, G. Why does the B3LYP hybrid functional fail for metals? *J. Chem. Phys.* **2007**, *127*, No. 024103.

(17) Perdew, J. P.; Ruzsinszky, A.; Csonka, G. I.; Vydrov, O. A.; Scuseria, G. E.; Constantin, L. A.; Zhou, X.; Burke, K. Restoring the Density-Gradient Expansion for Exchange in Solids and Surfaces. *Phys. Rev. Lett.* **2008**, *100*, 136406.

(18) Sun, J.; Ruzsinszky, A.; Perdew, J. Strongly Constrained and Appropriately Normed Semilocal Density Functional. *Phys. Rev. Lett.* **2015**, *115*, 036402.

(19) Chen, M.; Ko, H.-Y.; Remsing, R. C.; Andrade, M. F. C.; Santra, B.; Sun, Z.; Selloni, A.; Car, R.; Klein, M. L.; Perdew, J. P.; et al. Ab initio theory and modeling of water. *Proc. Natl. Acad. Sci. U. S. A.* **2017**, *114*, 10846.

(20) Sun, J.; Remsing, R. C.; Zhang, Y.; Sun, Z.; Ruzsinszky, A.; Peng, H.; Yang, Z.; Paul, A.; Waghmare, U.; Wu, X.; et al. Accurate first-principles structures and energies of diversely bonded systems from an efficient density functional. *Nat. Chem.* **2016**, *8*, 831−836.

(21) DelloStritto, M.; Piontek, S. M.; Klein, M. L.; Borguet, E. Relating Interfacial Order to Sum Frequency Generation with Ab Initio Simulations of the Aqueous $Al_2O_3(0001)$ and $(11\bar{2}0)$ Interfaces. *J. Phys. Chem. C* **2018**, *122*, 21284−21294.

(22) Ohto, T.; Usui, K.; Hasegawa, T.; Bonn, M.; Nagata, Y. Toward ab initio molecular dynamics modeling for sum-frequency generation spectra; an efficient algorithm based on surface-specific velocity-velocity correlation function. *J. Chem. Phys.* **2015**, *143*, 124702.

(23) Carroll-Webb, S. A.; Walther, J. V. A surface complex reaction model for the pH-dependence of corundum and kaolinite dissolution rates. *Geochim. Cosmochim. Acta* **1988**, *52*, 2609−2623.

(24) Wieland, E.; Wehrli, B.; Stumm, W. The coordination chemistry of weathering: III. A generalization on the dissolution rates of minerals. *Geochim. Cosmochim. Acta* **1988**, *52*, 1969−1981.

(25) Elam, J. W.; Nelson, C. E.; Cameron, M. A.; Tolbert, M. A.; George, S. M. Adsorption of H_2O on a Single-Crystal α-$Al_2O_3(0001)$ Surface. *J. Phys. Chem. B* **1998**, *102*, 7008−7015.

(26) Hass, K. C.; Schneider, W. F.; Curioni, A.; Andreoni, W. First-Principles Molecular Dynamics Simulations of H_2O on α-Al_2O_3 (0001). *J. Phys. Chem. B* **2000**, *104*, 5527−5540.

(27) Ma, S.-Y.; Liu, L.-M.; Wang, S.-Q. Water Film Adsorbed on the α-$Al_2O_3(0001)$ Surface: Structural Properties and Dynamical Behaviors from First-Principles Molecular Dynamics Simulations. *J. Phys. Chem. C* **2016**, *120*, 5398−5409.

(28) Tuladhar, A.; Piontek, S. M.; Frazer, L.; Borguet, E. Effect of Halide Anions on the Structure and Dynamics of Water Next to an Alumina (0001) Surface. *J. Phys. Chem. C* **2018**, *122*, 12819−12830.

(29) Dreier, L. B.; Nagata, Y.; Lutz, H.; Gonella, G.; Hunger, J.; Backus, E. H. G.; Bonn, M. Saturation of charge-induced water alignment at model membrane surfaces. *Science Advances* **2018**, *4*, eaap7415.

DOI: 10.1021/acs.jpclett.9b00016
J. Phys. Chem. Lett. 2019, 10, 2031−2036

(30) Huang, P.; Pham, T. A.; Galli, G.; Schwegler, E. Alumina-(0001)/Water Interface: Structural Properties and Infrared Spectra from First-Principles Molecular Dynamics Simulations. *J. Phys. Chem. C* **2014**, *118*, 8944−8951.
(31) DelloStritto, M.; Sofo, J. Bond Polarizability Model for Sum Frequency Generation at the $Al_2O_3(0001)H_2O$ Interface. *J. Phys. Chem. A* **2017**, *121*, 3045−3055.
(32) Tuladhar, A.; Piontek, S. M.; Borguet, E. Insights on Interfacial Structure, Dynamics, and Proton Transfer from Ultrafast Vibrational Sum Frequency Generation Spectroscopy of the Alumina(0001)/Water Interface. *J. Phys. Chem. C* **2017**, *121*, 5168−5177.
(33) Catalano, J. G. Weak interfacial water ordering on isostructural hematite and corundum (001) surfaces. *Geochim. Cosmochim. Acta* **2011**, *75*, 2062−2071.
(34) *Materials Studio*; Dassault Systèmes BIOVIA: San Diego, CA, 2016.
(35) Kirsch, H.; Wirth, J.; Tong, Y.; Wolf, M.; Saalfrank, P.; Campen, R. K. Experimental Characterization of Unimolecular Water Dissociative Adsorption on α-Alumina. *J. Phys. Chem. C* **2014**, *118*, 13623−13630.
(36) Martínez, L.; Andrade, R.; Birgin, E. G.; Martínez, J. M. PACKMOL: A package for building initial configurations for molecular dynamics simulations. *J. Comput. Chem.* **2009**, *30*, 2157−2164.
(37) Cygan, R. T.; Liang, J.-J.; Kalinichev, A. G. Molecular Models of Hydroxide, Oxyhydroxide, and Clay Phases and the Development of a General Force Field. *J. Phys. Chem. B* **2004**, *108*, 1255−1266.
(38) Plimpton, S. Fast Parallel Algorithms for Short-Range Molecular Dynamics. *J. Comput. Phys.* **1995**, *117*, 1−19.
(39) Argyris, D.; Ho, T.; Cole, D. R.; Striolo, A. Molecular Dynamics Studies of Interfacial Water at the Alumina Surface. *J. Phys. Chem. C* **2011**, *115*, 2038−2046.
(40) Skelton, A. A.; Fenter, P.; Kubicki, J. D.; Wesolowski, D. J.; Cummings, P. T. Simulations of the Quartz$(10\bar{1}1)$/Water Interface: A Comparison of Classical Force Fields, Ab Initio Molecular Dynamics, and X-ray Reflectivity Experiments. *J. Phys. Chem. C* **2011**, *115*, 2076−2088.
(41) Dewan, S.; Carnevale, V.; Bankura, A.; Eftekhari-Bafrooei, A.; Fiorin, G.; Klein, M. L.; Borguet, E. Structure of Water at Charged Interfaces: A Molecular Dynamics Study. *Langmuir* **2014**, *30*, 8056−8065.
(42) Tkatchenko, A.; Scheffler, M. Accurate Molecular Van Der Waals Interactions from Ground-State Electron Density and Free-Atom Reference Data. *Phys. Rev. Lett.* **2009**, *102*, 073005.
(43) Krukau, A. V.; Vydrov, O. A.; Izmaylov, A. F.; Scuseria, G. E. Influence of the exchange screening parameter on the performance of screened hybrid functionals. *J. Chem. Phys.* **2006**, *125*, 224106.
(44) DiStasio, R. A.; Santra, B.; Li, Z.; Wu, X.; Car, R. The individual and collective effects of exact exchange and dispersion interactions on the ab initio structure of liquid water. *J. Chem. Phys.* **2014**, *141*, 084502.
(45) Forster-Tonigold, K.; Groß, A. Dispersion corrected RPBE studies of liquid water. *J. Chem. Phys.* **2014**, *141*, No. 064501.
(46) Gillan, M. J.; Alfè, D.; Michaelides, A. Perspective: How good is DFT for water? *J. Chem. Phys.* **2016**, *144*, 130901.
(47) Kresse, G.; Hafner, J. Ab initio molecular-dynamics simulation of the liquidmetalamorphous-semiconductor transition in germanium. *Phys. Rev. B: Condens. Matter Mater. Phys.* **1994**, *49*, 14251−14269.
(48) Kresse, G.; Hafner, J. *Ab initio* molecular dynamics for liquid metals. *Phys. Rev. B: Condens. Matter Mater. Phys.* **1993**, *47*, 558−561.
(49) Kresse, G.; Furthmüller, J. Efficient iterative schemes for ab initio total-energy calculations using a plane-wave basis set. *Phys. Rev. B: Condens. Matter Mater. Phys.* **1996**, *54*, 11169−11186.
(50) Kresse, G.; Joubert, D. From ultrasoft pseudopotentials to the projector augmentedwave method. *Phys. Rev. B: Condens. Matter Mater. Phys.* **1999**, *59*, 1758−1775.
(51) Blöchl, P. E. Projector augmented-wave method. *Phys. Rev. B: Condens. Matter Mater. Phys.* **1994**, *50*, 17953−17979.
(52) Vanderbilt, D. Optimally smooth norm-conserving pseudopotentials. *Phys. Rev. B: Condens. Matter Mater. Phys.* **1985**, *32*, 8412−8415.
(53) Catalano, J. G. Relaxations and Interfacial Water Ordering at the Corundum (110) Surface. *J. Phys. Chem. C* **2010**, *114*, 6624−6630.
(54) Zhang, L.; Tian, C.; Waychunas, G. A.; Shen, Y. R. Structures and Charging of α-Alumina (0001)/Water Interfaces Studied by Sum-Frequency Vibrational Spectroscopy. *J. Am. Chem. Soc.* **2008**, *130*, 7686−7694.
(55) Gaigeot, M.-P.; Sprik, M.; Sulpizi, M. Oxide/water interfaces: how the surface chemistry modifies interfacial water properties. *J. Phys.: Condens. Matter* **2012**, *24*, 124106.
(56) Braunschweig, B.; Eissner, S.; Daum, W. Molecular Structure of a Mineral/Water Interface: Effects of Surface NanoRoughness of α-Al_2O_3 (0001). *J. Phys. Chem. C* **2008**, *112*, 1751−1754.
(57) Tuladhar, A.; Dewan, S.; Kubicki, J. D.; Borguet, E. Spectroscopy and Ultrafast Vibrational Dynamics of Strongly Hydrogen Bonded OH Species at the α-$Al_2O_2(11\bar{2}20)/H_2O$ Interface. *J. Phys. Chem. C* **2016**, *120*, 16153−16161.
(58) Bokdam, M.; Lahnsteiner, J.; Ramberger, B.; Schäfer, T.; Kresse, G. Assessing Density Functionals Using Many Body Theory for Hybrid Perovskites. *Phys. Rev. Lett.* **2017**, *119*, 145501.

DOI: 10.1021/acs.jpclett.9b00016
J. Phys. Chem. Lett. 2019, 10, 2031−2036